Aging Cell (2013) **12**, pp102–111 Doi: 10.1111/acel.12023

Increased dosage of *Ink4/Arf* protects against glucose intolerance and insulin resistance associated with aging

Herminia González-Navarro,[1]* Ángela Vinué,[2]* María Jesús Sanz,[1,3] Mercedes Delgado,[4] Miguel Angel Pozo,[4] Manuel Serrano,[5] Deborah J. Burks[6] and Vicente Andrés[7]

[1]Institute of Health Research-INCLIVA, Valencia, 46010, Spain
[2]Vascular Biology Unit, Department of Molecular and Cellular Pathology and Therapy, Instituto de Biomedicina de Valencia (IBV), Spanish Council for Scientific Research (CSIC), Valencia, 46010, Spain
[3]Departamento de Farmacología, Universidad de Valencia-INCLIVA, Valencia, 46010, Spain
[4]CAI Cartografía Cerebral, Instituto Pluridisciplinar, Universidad Complutense de Madrid, Madrid, 28040, Spain
[5]Spanish National Cancer Research Center (CNIO), Madrid, 28029, Spain
[6]CIBER de Diabetes y Enfermedades Metabolicas (CIBERDEM), Centro de Investigación Príncipe Felipe (CIPF), Valencia, 46012, Spain
[7]Laboratory of Molecular and Genetic Cardiovascular Pathophysiology, Department of Epidemiology, Atherothrombosis and Imaging, Centro Nacional de Investigaciones Cardiovasculares (CNIC), Madrid, 28029, Spain

Summary

Recent genome-wide association studies have linked type-2 diabetes mellitus to a genomic region in chromosome 9p21 near the *Ink4/Arf* locus, which encodes tumor suppressors that are up-regulated in a variety of mammalian organs during aging. However, it is unclear whether the susceptibility to type-2 diabetes is associated with altered expression of the *Ink4/Arf* locus. In the present study, we investigated the role of *Ink4/Arf* in age-dependent alterations of insulin and glucose homeostasis using *Super-Ink4/Arf* mice which bear an extra copy of the entire *Ink4/Arf* locus. We find that, in contrast to age-matched wild-type controls, *Super-Ink4/Arf* mice do not develop glucose intolerance with aging. Insulin tolerance tests demonstrated increased insulin sensitivity in *Super-Ink4/Arf* compared with wild-type mice, which was accompanied by higher activation of the insulin receptor substrate (IRS)-PI3K-AKT pathway in liver, skeletal muscle and heart. Glucose uptake studies in *Super-Ink4/Arf* mice showed a tendency toward increased ^{18}F-fluorodeoxyglucose uptake in skeletal muscle compared with wild-type mice ($P = 0.079$). Furthermore, a positive correlation between glucose uptake and baseline glucose levels was observed in *Super-Ink4/Arf* mice ($P < 0.008$) but not in wild-type mice. Our studies reveal a protective role of the *Ink4/Arf* locus against the development of age-dependent insulin resistance and glucose intolerance.

Key words: ^{18}F-fluorodeoxyglucose-PET; ARF; CDKN2A; CDKN2B; diabetes; insulin resistance; insulin signaling; p15^{ink4b}; p16^{ink4a}; pancreatic islet.

Introduction

Patients with type 2 diabetes mellitus (T2DM) are at higher risk for developing cardiovascular disease and have a shorter lifespan compared with the general population (Benetos *et al.*, 2008). T2DM is increasing worldwide at alarming rates due to unhealthy lifestyles (e.g., lack of exercise, excessive caloric intake) and to population aging (Beckman *et al.*, 2002; Nunn *et al.*, 2009). It is well established that aged cells are more susceptible to the development of chronic diseases; however, the underlying molecular mechanisms are not completely understood (Sharpless & DePinho, 2007).

Both environmental and genetic factors play a major role in the etiopathogenesis of T2DM. Recent human genome-wide association studies and candidate gene approaches using large cohorts have linked common single nucleotide polymorphisms (SNPs) in a region of chromosome 9p21 in close vicinity to the *Ink4a/Arf/Ink4b* locus (hereby abbreviated as *Ink4/Arf*) with aging-associated frailty and a variety of aging-related diseases, including coronary artery disease, myocardial infarction, stroke, and T2DM (Consortium, 2007; Melzer *et al.*, 2007; Saxena *et al.*, 2007; Scott *et al.*, 2007; Sharpless & DePinho, 2007; Zeggini *et al.*, 2007; Doria *et al.*, 2008; Hamsten & Eriksson, 2008). The *Ink4/Arf* locus is one of the main anti-oncogenic defenses of mammalian cells and its loss is among the most frequent cytogenetic events in human cancer (Gil & Peters, 2006). *Ink4/Arf* encodes the tumor suppressors p16^{Ink4a} and ARF (p14^{ARF} in humans, p19^{Arf} in mice) (*CDKN2A* gene) and p15^{INK4b} (*CDKN2B* gene). In humans, the locus also contains the *CDKN2BAS* gene, which produces a noncoding antisense RNA named ANRIL (antisense noncoding RNA in the INK4 locus) that is thought to regulate *CDKN2A* and *CDKN2B* expression (reviewed in) (Cunnington & Keavney, 2011). p16^{Ink4a} and p15^{Ink4b} block cell proliferation through the inhibition of CDK4,6/cyclin D kinases and the ensuing accumulation of the hypophosphorylated form of the retinoblastoma protein (Vidal & Koff, 2000).

ARF appears to play a relevant role as a pro-apoptotic factor via inhibition of MDM2, an ubiquitin ligase that destabilizes the tumor suppressor p53 (Gonzalez & Serrano, 2006). Several studies in mice and humans have demonstrated an age-dependent increase of *Ink4/Arf* expression in different tissues, which might limit the regenerative potential of stem cell pools (Zindy *et al.*, 1997; Krishnamurthy *et al.*, 2004; Ressler *et al.*, 2006; Collado *et al.*, 2007). These observations have been generally interpreted as indicative of a pro-aging role for the *Ink4/Arf* locus. However, various lines of evidence indicate that maximal regenerative potential may be detrimental for the long-term maintenance of stem cell pools. For example, deletion of the tumor suppressors Lkb1, Pten, Apc, p21^{Cip1}, weakens stem cell quiescence and results in premature exhaustion of stem cell function (Kippin *et al.*, 2005; Zhang

Correspondence
Vicente Andrés, CNIC, Melchor Fernández Almagro 3, 28029 Madrid, Spain. Tel.: +34-914531200; fax: +34-914531265, e-mail: vandres@cnic.es;
Herminia González-Navarro, Fundación Investigación Hospital Clínico de Valencia-INCLIVA, Av. Blasco Ibáñez, 17, 46010, Valencia, Spain. Tel.: +34-96 386 28 94, fax: +34-96 398 78 60; e-mail: gonzaleh@uv.es

*These authors contributed equally to this work.

Abbreviations
^{18}F-FDG, ^{18} Fluor-Fluorodeoxyglucose; AKT, V-akt murine thymomaviral oncogene homolog kinase; AUC, area under the curve; CDK, cyclin-dependent kinase; GTT, glucose tolerance test; HDL-C, HDL-cholesterol; IRS, insulin receptor substrate; ITT, insulin tolerance test; PI3K, phosphatidylinositol-3 kinase; SNP, single nucleotide polymorphism; SUV, standard uptake value; T2DM, type 2 Diabetes Mellitus; VOI, volume of interest.

Accepted for publication *19 October 2012*

et al., 2006; Qian *et al.*, 2008; Gan *et al.*, 2010; Gurumurthy *et al.*, 2010). In this context, aging-induced *Ink4/Arf* expression could represent an anti-aging defensive response to prevent the exhaustion of stem cell pools. Indeed, *Ink4/Arf* gain-of-function in transgenic mice confers beneficial cancer-resistant phenotypes and elicits a global anti-aging effect (Matheu *et al.*, 2004, 2009). Moreover, $p16^{Ink4a}$ and $p19^{Arf}$ expression protects from atherosclerosis development in the mouse (Gonzalez-Navarro *et al.*, 2010; Kuo *et al.*, 2011). In further support of a beneficial effect of the *Ink4/Arf* locus on aging-associated diseases, in the case of the human SNP linked to atherosclerosis, the susceptibility allele is associated with lower levels of *Ink4/Arf* expression than the normal allele (Liu *et al.*, 2009). Thus, it remains to be established whether the *Ink4/Arf* locus is a general pro-aging gene, a general anti-aging gene, or, alternatively, whether its effects are tissue specific.

In the present study, we investigated the impact of increased dosage of *Ink4/Arf* on insulin and glucose homeostasis during normal physiological aging. To this end, we utilized transgenic *Super-Ink4/Arf* mice bearing an extra allele of the entire *Ink4/Arf* locus that behaves similarly to the endogenous gene, with minimal expression in primary embryonic cells and up-regulation in response to mitogenic overstimulation (Matheu *et al.*, 2004). Compared with wild-type *(WT)* controls, aged *Super-Ink4/Arf* mice display moderately increased levels of $p16^{Ink4}$, $p15^{Ink4b}$, and $p19^{Arf}$ in a number of tissues, yet they exhibit higher resistance to both chemically induced cancer and aging-associated spontaneous cancer (Matheu *et al.*, 2004, 2007). In the present work, we characterized carbohydrate metabolism and β-cell function in 0.5- and 1-year-old *Super-Ink4/Arf* mice and age-matched *WT* littermates. As defective signaling through insulin receptor substrate (IRS)-PI3K-AKT has been associated with T2DM and insulin resistance (Withers *et al.*, 1998; Cho *et al.*, 2001; Gonzalez-Navarro *et al.*, 2008), we also examined this pathway in both groups of mice.

Results

Ink4/Arf locus expression studies in *Super-Ink4/Arf* and *WT* mice

To analyze the role of the locus *Ink4/Arf* in age-associated glucose homeostasis, we first characterized gene expression in tissues relevant for carbohydrate metabolism in both transgenic *Super-Ink4/Arf* and *WT* mice. Fig. 1A depicts the structure of the transgene used to generate *Super-Ink4/Arf*, consisting of the entire *Ink4/Arf* locus under the control of its own promoter that behaves similarly to the endogenous gene (Matheu *et al.*, 2004). Quantification by qPCR showed a modest increase in $p16^{Ink4a}$, $p15^{Ink4b}$, and $p19^{Arf}$ mRNA expression in liver of *Super-Ink4/Arf* mice compared with *WT* mice, although differences were only statistically significant for $p15^{Ink4b}$ (Fig. 1B). In skeletal muscle, heart, and isolated islets, no significant differences in transcript levels were observed, and $p19^{Arf}$ was not detected in skeletal muscle (Fig. 1B). Protein expression analysis also revealed a modest but not significant increase in hepatic $p16^{Ink4a}$, $p15^{Ink4b}$, and $p19^{Arf}$ protein levels in *Super-Ink4/Arf* compared with *WT* mice (Fig. 1C). In agreement with our qPCR studies, Western blot analysis revealed no differences in skeletal muscle, heart, and isolated islets from mice of both genotypes (Fig. 1C). Despite modest changes in the expression of the gene products of the locus, *Super-InK4/Arf* macrophages showed a significant increase in apoptosis compared with *WT* controls (Fig. 1D), demonstrating an enhanced functionality of the extra dosage of the locus in transgenic animals.

Super-Ink4/Arf mice are protected against the age-associated decline of glucose homeostasis

To investigate the role of *Ink4/Arf* in carbohydrate metabolism associated with aging, *WT* and *Super-Ink4/Arf* mice were analyzed at 0.5 and 1 year of age. Body weight increased significantly with age in both *WT* and *Super-Ink4/Arf* mice, and no differences were observed between genotypes ($P > 0.05$) at any of the time points in our study (Fig. 2A). However, while fasting plasma glucose levels were undistinguishable between 0.5-year-old *WT* and *Super-Ink4/Arf* mice, glucose levels were significantly increased in 1-year-old *WT* mice but not in age-matched *Super-Ink4/Arf* mice (Fig. 2B). Aging also affected differentially fasting plasma insulin levels in mice of both genotypes. Thus, no differences were observed between 0.5-year-old *WT* and *Super-Ink4/Arf* mice, but insulin levels were lower in *Super-Ink4/Arf* mice at 1 year of age (Fig. 2C). Although altered glucose homeostasis and hypercholesterolemia (Nunn *et al.*, 2009) are often associated with aging, neither aging nor increased gene dosage of *Ink4/Arf* affected circulating levels of total cholesterol and HDL-cholesterol (Fig. 2D, E).

We next performed glucose tolerance tests (GTT) in fasted mice. Glucose tolerance, as revealed by the area under the curve (glucose curve *vs* time, $AUC_{glucose}$), was similar in 0.5-year-old *WT* and *Super-Ink4/Arf* mice (Fig. 3A). At 1 year of age, the $AUC_{glucose}$ increased significantly in *WT* as compared with 0.5-year-old mice but not in *Super-Ink4/Arf* mice (Fig. 3A). Likewise, analysis of the corresponding glucose-stimulated insulin release, expressed as $AUC_{insulin}$, revealed no differences between genotypes at 0.5 year of age, but we observed a significant decrease in 1-year-old *Super-Ink4/Arf* compared with *WT* mice of the same age (Fig. 3B). Thus, increased *Ink/Arf* gene dosage prevents the development of age-dependent deterioration of glucose metabolism, but this is not accompanied by enhanced insulin secretion. To investigate whether insulin sensitivity was affected in these mice, we performed insulin tolerance tests (ITT) in 0.5- and 1-year-old mice of both genotypes (Fig. 3C). These studies revealed faster glucose disappearance in *Super-Ink4/Arf* mice compared with *WT* mice after insulin injection, suggesting that increased *Ink4/Arf* gene dosage augments insulin sensitivity.

To evaluate the effect of increased insulin sensitivity on in vivo glucose disposal and uptake, we performed ^{18}F-fluorodeoxyglucose (^{18}F-FDG) Positron Emission Tomography (PET)–Computer Tomography (CT) imaging studies. To this end, 1-year-old mice were intraperitoneally injected with ^{18}F-FDG and after 60 minutes of uptake, skeletal muscle was analyzed by PET–CT imaging (Fig. 4A). Quantification of the standard uptake value (SUV) showed an almost significant increase in^{18}F-FDG uptake in soleus muscle from *Super-Ink4/Arf* mice compared with *WT* mice (Fig. 4B, $P = 0.079$). Furthermore, regression analysis demonstrated a positive correlation between ^{18}F-FDG uptake and baseline glucose levels in *Super-Ink4/Arf* mice but not in *WT* mice (Fig. 4C), suggesting that *WT* mice are insensitive to glucose levels.

Super-Ink4/Arf mice exhibit increased insulin sensitivity in liver and peripheral tissues

To further characterize insulin sensitivity in age-associated glucose and insulin derangements in *WT* and *Super-Ink4/Arf* mice, we analyzed insulin signaling pathway activation *in vivo*. Insulin exerts its actions through binding to its receptor (INS-R) and the ensuing phosphorylation of IRS at tyrosine residues (pTyr) and activation of PI3K/AKT-dependent signaling. As ablation or defective INS-R/IRS/AKT-mediated signaling in a variety of

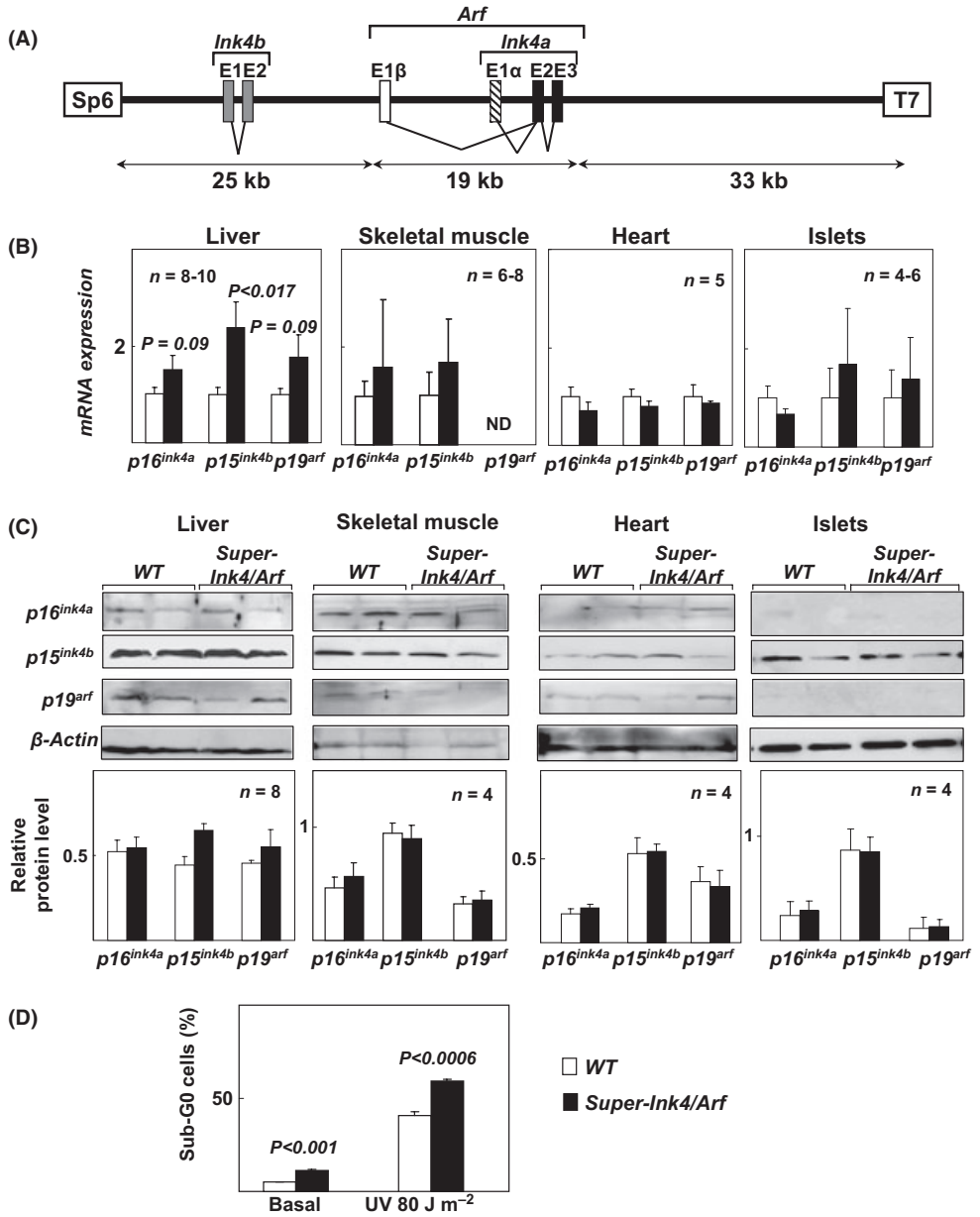

Fig. 1 *Ink4/Arf* locus expression and function in 1-year-old *Super-Ink4/Arf* and WT mice. (A) Structure of the transgene used for the generation of *Ink4/Arf* transgenic mice. The transgene contains the complete exon structure of the three genes, *Ink4b*, *Arf,* and *Ink4a*. Boxes labeled SP6 and T7 represent short terminal sequences (of 20 bp) used for the identification of the transgene by PCR. (B) $p16^{Ink4a}$, $p15^{Ink4b}$, and $p19^{Arf}$ mRNA expression in liver, skeletal muscle, heart, and isolated pancreatic islets quantified by qPCR. mRNA levels were normalized to endogenous cyclophilin levels and relativized to *WT* mRNA levels (=1). N.D.: not detected. (C) Protein lysates (liver, skeletal muscle, heart: 250 μg; isolated islets: 75 μg) were subjected to Western blot analysis using antibodies against $p16^{Ink4a}$, $p15^{Ink4b}$, $p19^{Arf}$, and β-actin. Representative blots are shown and quantifications in the graphs represent the average of 4-8 independent blots. Protein levels were normalized to β-actin levels. (D) Bone-marrow-derived macrophages were untreated (basal) or irradiated with UV light (80 J/m^2) to induce apoptosis. After propidium iodide staining, apoptotic cells were identified by flow cytometry as the sub-G0 population. Statistical analysis was carried out using two-way ANOVA (B, C) and Student's *t*-test (D).

tissues causes major alterations in glucose homeostasis and leads to insulin resistance and T2DM (Withers *et al.*, 1998; Cho *et al.*, 2001; Gonzalez-Navarro *et al.*, 2007, 2008) we analyzed IRS-AKT pathway activation in liver and peripheral tissues of 1-year-old *WT* and *Super-Ink4/Arf* mice treated with insulin. Coimmunoprecipitation experiments followed by Western blot analysis revealed reduced levels of insulin-induced pTyr-IRS1 and pTyr-IRS2 accumulation in *WT* compared with *Super-Ink4/Arf* liver (Figure 5A, B). IRS1 or IRS2 associated with the PI3K regulatory subunit p85α was similar in the liver of insulin-stimulated *WT* and Super-Ink4/*Arf* mice (Fig. 5A, B). Analysis of hepatic IRS1 and IRS2 protein and mRNA levels showed no differences between genotypes (Fig. 5C).

We next examined in peripheral tissues of 1-year-old mice the activation of AKT1/2 using a phospho-specific antibody to detect phospho-AKT1/2 (pAKT1/2). Consistent with our results in liver, we found diminished amount of insulin-stimulated pAKT1/2 in skeletal muscle and heart of *WT* compared with *Super-Ink4/Arf* mice, without

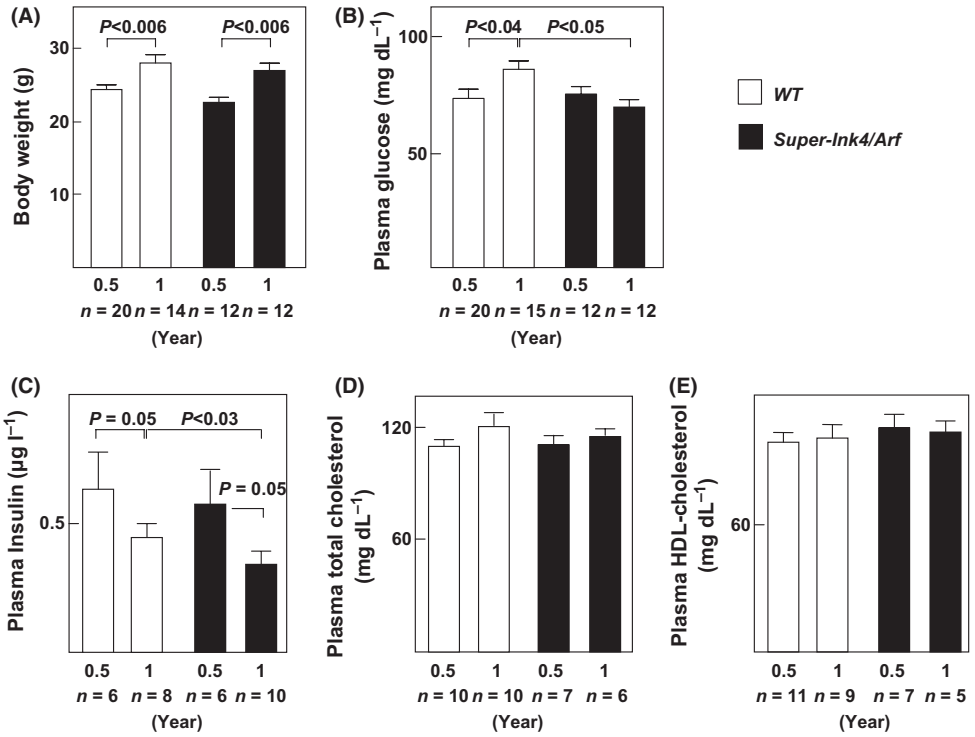

Fig. 2 Effect of increased gene dosage of *Ink4/Arf* on plasmatic glucose, insulin, and cholesterol. (A) Body weight of *WT* and *Super-Ink4/Arf* mice of the indicated ages. Mice were fasted overnight to measure plasma glucose (B), insulin (C), and cholesterol (D, E). Statistical analysis was performed using one-way ANOVA.

changes in total AKT1/2 (Fig. 6). As enhanced basal activation of JNK has been associated with decreased IRS1 in insulin resistance (Hirosumi *et al.*, 2002), we examined the phosphorylation status of this mitogen-activated protein kinase. However, the amount of pJNK was similar in control and insulin-stimulated skeletal muscle (Fig. 6A) and heart (Fig. 6B) of *WT* and *Super-Ink4/Arf* mice. Altogether, these results indicate that improved insulin sensitivity in liver and peripheral tissues contributes to protection against age-associated glucose and insulin derangements in *Super-Ink4/Arf* mice.

Discussion

Recent human genome-wide association studies and candidate gene strategies have linked common single nucleotide polymorphisms in a region of chromosome 9p21 near the *Ink4/Arf* locus with aging-associated diseases which have an important impact on public health, including coronary artery disease, myocardial infarction, stroke, and T2DM (Consortium, 2007; Melzer *et al.*, 2007; Saxena *et al.*, 2007; Scott *et al.*, 2007; Sharpless & DePinho, 2007; Zeggini *et al.*, 2007; Doria *et al.*, 2008; Hamsten & Eriksson, 2008). However, additional work is required to define the functional consequences of these genetic variants and to ascertain whether *Ink4/Arf* plays a role in the development of cardiovascular disease and T2DM associated with aging. In the present study, we evaluated the impact of moderately increasing *Ink4/Arf* expression on glucose and insulin homeostasis during normal aging. Our results demonstrate that transgenic *Super-Ink4/Arf* mice carrying one intact additional copy of the *Ink4/Arf* locus are protected against the aging-associated alterations in glucose homeostasis normally seen in *WT* mice, including increased glycaemia, glucose intolerance, and insulin resistance. This protective function of *Ink4/Arf* gain-of-function was not associated with changes in either islet number, pancreatic β-cell area, or β-cell proliferation (Figure S1), but coincided with increased sensitivity to insulin in peripheral tissues. Our results demonstrate that insulin-stimulated activation of IRS-PI3K-AKT-dependent signaling was greater in liver, skeletal muscle, and heart of *Super-Ink4/Arf* mice than in *WT* controls. In agreement with enhanced insulin sensitivity and signaling and lower glucose levels, *Super-Ink4/Arf* mice exhibited an almost significant increase in glucose uptake in skeletal muscle compared with *WT* mice. Furthermore, a positive correlation between glucose uptake and baseline glucose levels was observed in *Super-Ink4/Arf* but not in *WT* mice. Taken together, our results suggest that a moderate increase in *Ink4/Arf* function prevents age-associated derangements in glucose metabolism and insulin resistance by improving insulin-dependent activation of IRS-PI3K-AKT signaling. In agreement with previous studies showing that *Ink4/Arf* expression is low in young animals and increases in several tissues during aging (reviewed in (Krishnamurthy *et al.*, 2004)) and that *Ink4/Arf* expression is only moderately upregulated in tissues from ~1.5-year-old *Super-Ink4/Arf* mice (Matheu *et al.*, 2004), we only observed a modest increase in *Ink4/Arf* mRNA and protein levels in the liver of 1-year-old *Super-Ink4/Arf* mice (Fig. 1B, C). Importantly, however, this modest upregulation has functional consequences, as demonstrated by higher UV-induced apoptosis in *Super-Ink4Arf* bone-marrow-derived macrophages (Fig. 1D).

Aging is associated with augmented susceptibility to the development of T2DM and other metabolic diseases (Rhodes, 2005), and with increased expression of *Ink4/Arf* in several human and mouse tissues (Zindy *et al.*, 1997; Krishnamurthy *et al.*, 2004; Ressler *et al.*, 2006). In addition to promoting senescence of somatic cells, age-dependent up-regulation of *Ink4/Arf* might contribute to organismal aging by limiting the regenerative potential of stem cell pools (Krishnamurthy *et al.*, 2004). Importantly, Baker *et al.* recently reported that clearance of $p16^{Ink4a}$-positive senescent cells delays aging-associated disorders in the

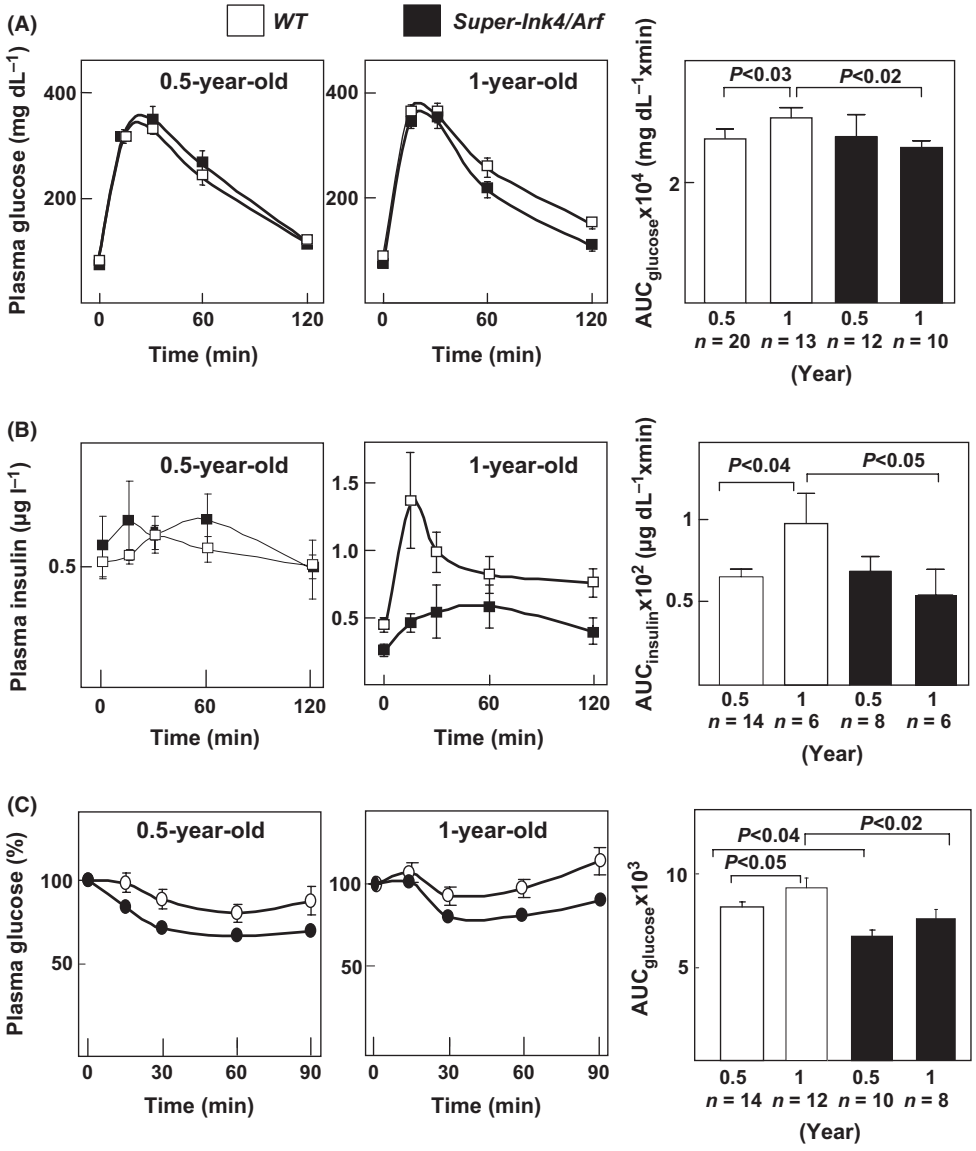

Fig. 3 Increased gene dosage of *Ink4/Arf* improves glucose tolerance and insulin sensitivity in mice. (A, B) Glucose tolerance test (GTT) was performed in 0.5- and 1-year-old *WT* and *Super-Ink4/Arf* mice. The graphs show the plasmatic levels of glucose (A) and insulin (B) at the different time points analyzed during the test. These values were used to calculate the area under the curve (AUC) (shown in the graphs in the right). (C) ITTs were performed in 0.5- and 1-year-old mice 4 h after food removal. The graphs in the left show levels of glucose at different time points analyzed during the test (relative to initial glucose level). The graph in the right depicts the AUCs. Statistical analysis was performed using one-way ANOVA.

BubR1 progeroid mouse background (Baker *et al.*, 2008). However, evidence exists that *Ink4/Arf* can also elicit beneficial effects. Thus, *Super-Ink4/Arf* mice, which carry one extra copy of *Ink4/Arf* and exhibit a moderate increase in $p16^{Ink4a}$, $p15^{Ink4b}$, and $p19^{Arf}$ expression in a number of tissues at old ages, are more resistant to cancer than controls and have normal aging and lifespan (Matheu *et al.*, 2004). Moreover, introduction of two intact additional copies of the *Ink4/Arf* locus in transgenic mice increases cancer resistance and extends lifespan probably by favoring quiescence and preventing unnecessary cell proliferation (Matheu *et al.*, 2009). The *Ink4/Arf* locus also exerts atheroprotective functions, because increased atherosclerosis was observed in apolipoprotein-E deficient mice with global ablation of $p19^{Arf}$ (Gonzalez-Navarro *et al.*, 2010) and in LDL-receptor-deficient mice with macrophage-specific deficiency of the *CDKN2A* gene, which encodes $p16^{Ink4a}$ and $p19^{Arf}$ (Kuo *et al.*, 2011). The results of the present study provide additional evidence that this locus can exert beneficial effects at the organismal level beyond cancer protection.

Aging in humans and mice is associated with loss of insulin sensitivity and hyperinsulinemia (Rhodes, 2005). Moreover, impaired signaling through INS-R/IRS/AKT in a variety of tissues (including β-cells, adipocytes, leukocytes, hepatocytes) leads to insulin resistance and T2DM (Withers *et al.*, 1998; Cho *et al.*, 2001; Gonzalez-Navarro *et al.*, 2007, 2008). Consistent with these results, we observed that glucose tolerance declines in 1-year-old *WT* but not in age-matched *Super-Ink4/Arf* mice. This is explained, at least in part, because insulin-mediated activation of IRS-PI3K-AKT signaling in liver, skeletal muscle, and heart is enhanced as compared with age-matched control mice. This augmented signaling was accompanied by increased glucose

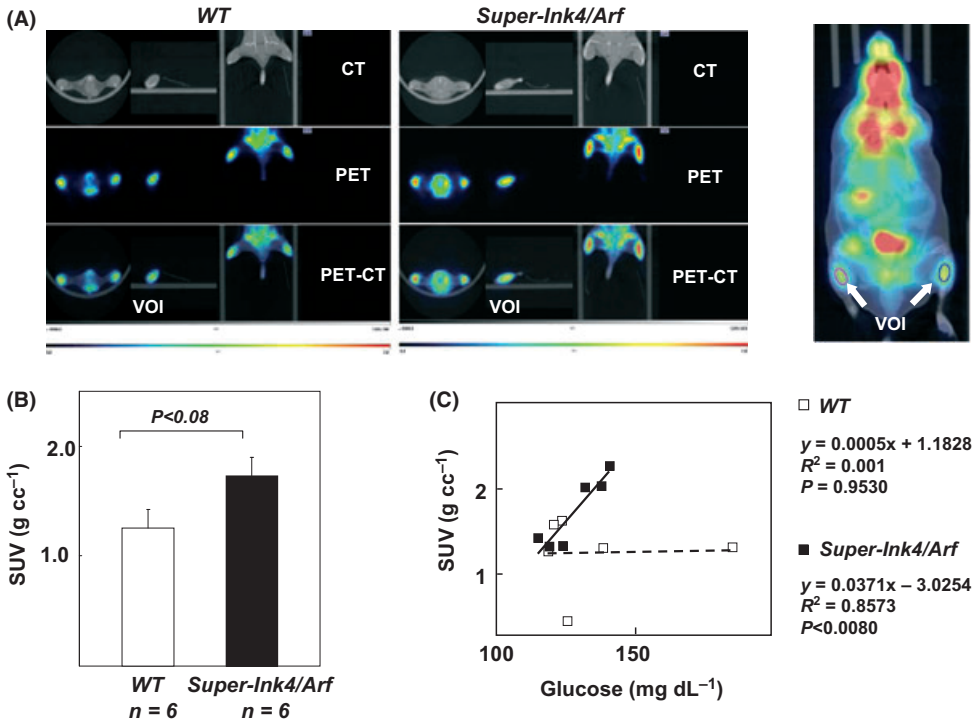

Fig. 4 Effect of the increased dosage of the locus *Ink4/Arf* on ^{18}F-FDG uptake in skeletal muscle *in vivo*. (A) Representative scans from *WT* and *Super-Ink4/Arf* mice showing transaxial images of the lower section of the mouse body (Top: CT, middle: PET; bottom: fused PET/CT). The image in the right shows whole-body PET. Lines in the image delineate the VOI in the soleus muscle used for analysis. (B) ^{18}F- FDG uptake in soleus muscle measured by PET scan. (C) Regression analysis of ^{18}F- FDG uptake (SUV) as a function of blood glucose levels. Each point represents one animal. Statistical analysis was performed using t-test (B) or F-test (C).

uptake in skeletal muscle and decreased glucose levels in *Super-Ink4/Arf* mice. Our studies suggest that a moderate increase in *Ink4/Arf* function may represent a logical target for treating or delaying age-related development of insulin resistance and carbohydrate metabolism derangement.

It has been shown that HOMA-IR in patients is strongly modulated by variants in *CDKN2B* (Ruchat *et al.*, 2009). However, some studies suggest that the 9p21 SNPs are associated with reduced islet function, such as decreased insulin secretion (Ruchat *et al.*, 2009; Stancakova *et al.*, 2009 Hribal *et al.*, 2011), and not with differences in insulin resistance (Hribal *et al.*, 2011) and body mass (Hotta *et al.*, 2012). We found that moderately increased expression of the entire *Ink4/Arf* locus in *Super-Ink4/Arf* mice does not alter islet number, β-cell area, or functionality during physiological aging (Figure S1), but rather appears to protect against age-associated glucose intolerance and insulin resistance. However, previous studies have shown that deficiency in $p16^{ink4a}$ enhances islet proliferation and survival in mice with streptozotocin-induced β-cell ablation. Moreover, $p16^{ink4a}$ overexpression decreases islet proliferation suggesting that increase of $p16^{ink4a}$ expression might limit the regenerative capacity of β-cells (Krishnamurthy *et al.*, 2006). It should be noted that streptozotocin treatment, a model of Type 1 diabetes, probably involves acute mitogenic stimulation and high level of $p16^{ink4a}$ expression, which has been shown to occur during regeneration after acute damage of a variety of tissues such as fat, skeletal muscle, hematopoietic system, nervous system, and endocrine pancreas (Janzen *et al.*, 2006; Krishnamurthy *et al.*, 2006; Molofsky *et al.*, 2006; Baker *et al.*, 2008). However, this might not be predictive of the long-term consequences of moderately increased $p16^{ink4a}$ in nonacute models, such as in the studies reported here. Our observations that *Super-Ink4/Arf* mice do not exhibit alterations in islet number, β-cell area, or functionality during physiological aging are not unprecedented, as Kir6.2, a component of the K-ATP channels that promotes insulin secretion in β-cells, is a direct target of E2F1 (Annicotte *et al.*, 2009). These results suggest that both the *Ink4/Arf* and CDK4–pRB–E2F1 pathways regulate glucose homeostasis without affecting β-cell proliferation. Additional studies using loss-of-function and tissue-specific genetic manipulation in the mouse should address the impact of $p16^{ink4a}$, $p19^{Arf}$, and $p15^{ink4b}$ on islet function during aging in order to dissect the precise contributions of the *Ink4/Arf* locus to glucose homeostasis and insulin sensitivity.

Experimental procedures

Mice

Care of animals was in accordance with institutional guidelines and regulations. Transgenic *Super-Ink4/Arf* mice used in this study carried one extra copy of the entire *Ink4/Arf* locus, which consisted of a 77 kb sequence that contained the complete exon structure flanked with two 20 bp short nucleotide sequences used for the identification of the transgene by PCR (Matheu *et al.*, 2004) (Fig. 1A). Transgenic mice were obtained after 20 backcrosses into C57BL6 background and were heterozygous for the additional *Ink4/Arf* locus. Siblings obtained by crossing C57BL6 *WT* and *SuperInk4Arf* mice were analyzed. Mice were genotyped for the presence of the extra *Ink4/Arf* gene dosage using two independent PCR reactions as previously described (Matheu *et al.*, 2004). Mice were kept on a low-fat standard diet (2.8% fat; Panlab, Barcelona, Spain) and sacrificed at 0.5 (mice between 5–7 months of age) or 1 year of age (mice between 11–13 months of age).

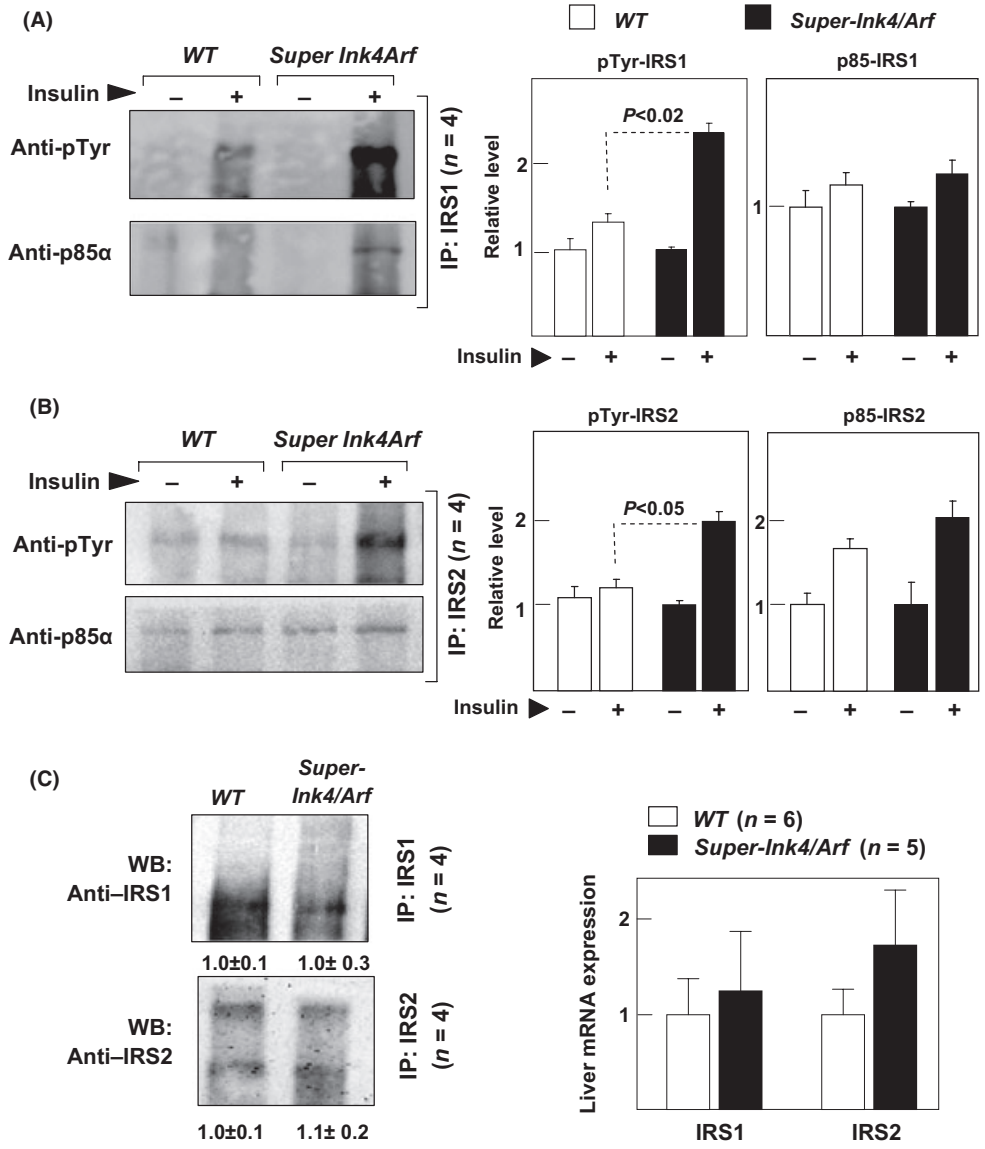

Fig. 5 Augmented gene dosage of *Ink4/Arf* increases insulin-induced signaling in the liver of 1-year-old mice. (A, B) Fasted mice were treated with insulin and sacrificed after 5 min to prepare liver protein lysates, which were subjected to immunoprecipitation with anti-IRS1 (A) or anti-IRS2 (B) antibodies and analyzed by western blot using anti-phospho-tyrosine (anti-pTyr) or anti-p85α antibodies. Representative blots are shown on the left. The graphs show relative levels of expression (average of 4 independent blots) (protein levels were relativized to unstimulated mice of the same genotype). (C) IRS1 and IRS2 protein (left) and mRNA (right) expression in liver. Liver protein lysates were subjected to immunoprecipitation with anti-IRS1 or anti-IRS2 antibodies and analyzed by western blot (WB). Representative blots are shown. The numbers below each blot show band intensity determined by densitometry after averaging 4 independent experiments (relative to *WT* mice). mRNA levels were normalized to *cyclophilin* mRNA levels and relativized to *WT* mouse expression.

Metabolic measurements

Plasma cholesterol levels in mice fasted overnight were measured using enzymatic procedures (Wako, St. Louis, USA). HDL-cholesterol (HDL-C) was determined after precipitation of the apoB-containing lipoproteins with Heparin Calcium (Sigma, St. Louis, MI, USA) (Gonzalez-Navarro *et al.*, 2007). For GTTs, mice received an intraperitoneal injection of glucose (2 g/Kg of body weight; Sigma) and plasma glucose and insulin levels were analyzed at different time points using a glucometer (Ascensia Elite, Bayer, Leverkusen, Germany) and ultrasensitive anti-mouse insulin ELISA (Mercodia, Uppsala, Sweden), respectively. For ITTs, mice fasted for 4 h received an intraperitoneal injection of insulin (Actrapid, Novo Nordisk, Madrid, Spain, 0.25 U/Kg of body weight), and plasma glucose levels were measured from tail blood at different time points using a glucometer.

In vivo insulin signaling studies

Anesthetized fasted mice (15 h) were injected with Humulina Regular (Lilly, Indianapolis, IN, USA, 0.25 U of insulin/g of BW) in the hepatic vein and killed 5 min later. Liver, skeletal muscle, and heart were removed and rapidly frozen in liquid N2 for protein extraction. Two mice per genotype were stimulated, and Western blot analysis was performed in quadruplicate.

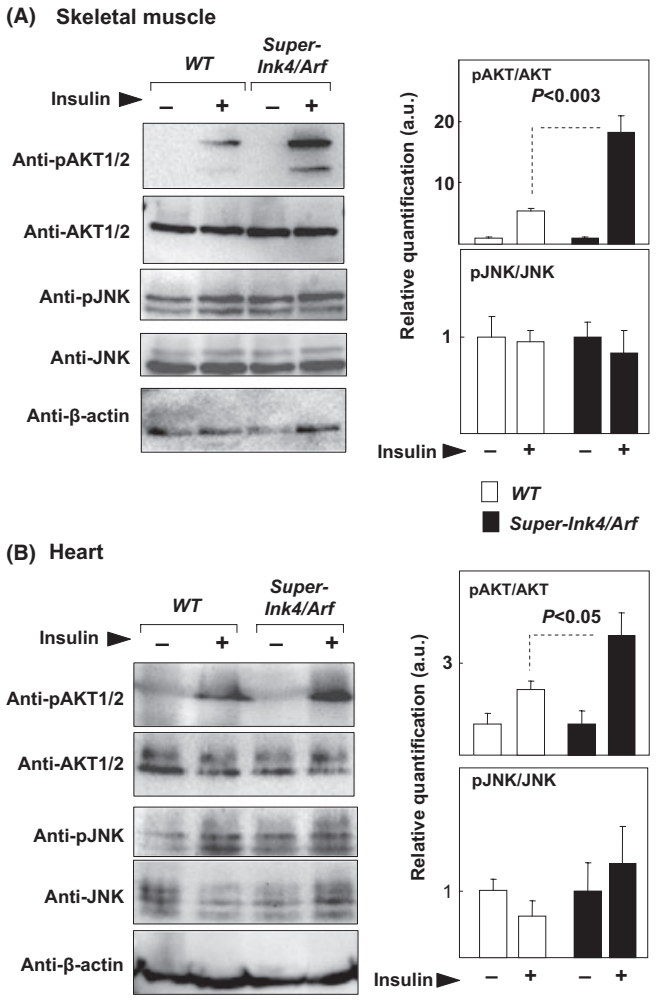

Fig. 6 Increased gene dosage of *Ink4/Arf* improves peripheral insulin signaling in 1-year-old mice. Fasted mice were treated with insulin and sacrificed after 5 min to prepare skeletal muscle (A) and heart (B) protein lysates, which were subjected to Western blot analysis using antibodies against phospho-AKT1/2 (pAKT1/2), AKT1/2, phospho-JNK (pJNK), JNK, and β-actin. Representative blots are shown on the left. The graphs show relative levels of expression (average of 4 independent blots). Phosphorylated (active) forms of each protein were normalized to total protein levels and are shown relative to unstimulated mice of the same genotype.

In vivo PET–CT imaging to study ^{18}F-FDG skeletal muscle uptake

Nonfasted mice were injected intraperitoneally with 11.1 MBq (300 of μCi in 0.2 mL of 0.9% NaCl) of the radiotracer ^{18}F-FDG. After an uptake period of 60 min, mice were anesthetized (2% isofluorane) to assure immobilization during the scanning process and placed on the bed of the tomography. PET acquisition was performed during 20 min, followed by a CT scanning using a specific small animal PET–CT hybrid tomograph (Albira ARS, Oncovision, Valencia, Spain) with an image resolution of <1.5 mm and a 8-cm transaxial, and a 4-cm axial field of view. The tomographic images were reconstructed by applying an ordered subset expectation maximization algorithm for the PET and a filtered back projection for the CT images. To evaluate ^{18}F-FDG uptake in the skeletal muscle, the volume of interest (VOI) was delineated around the soleus muscle, which consisted of 8 consecutive piled ellipse of 0.0125 mm thickness. The VOIs were then transferred to PET–CT coregistered images to obtain the average activity of the soleus FDG uptake (kBq/cc). For quantification purposes, the SUV was calculated as a ratio of tissue radioactivity concentration (kBq/cc) at the time of PET acquisition and injected dose (KBq) divided by body weight (g). All these processes of visualization, coregistration and quantification were performed using the PMOD 3.0 suite (Pmod Technologies, Zurich, Switzerland).

Isolation of pancreatic islets

For islet isolation, mice were infused with Krebs buffer (127mM NaCl, 5 mM KCl, 3 mM $CaCl_2$, 1.5 mM $MgCl_2$, 24 mM $NaHCO_3$, 6 mM Hepes, 2 mg/mL glucose, 0.1% albumin, equilibrated with 5% CO_2 in O_2). Pancreas were dissected from mice and digested with collagenase-NB8 (1 mg/mL, 17456, Serva, Heidelberg, Germany) in Krebs solution at 37 °C in a shaking water bath during 20 min. After washing with Krebs (800 g, 1 min), islets were handpicked under stereoscope, collected (500 g, 1 min) and frozen with liquid N_2 for RNA and protein analysis.

Coimmunoprecipitation and western blot analysis

Protein extracts were obtained from different tissues using a homogenizer in the presence of the ice-cold lysis TNG buffer (50 mM Tris-HCl, pH7.5, 200 mM NaCl, 1% Tween-20, 0.2% NP-40) supplemented with Complete Mini cocktail (Roche, Mannheim, Germany), 50 mM ß-glycerolphosphate (Sigma), 2 mM PhenylMethylSulfonyl Fluorid (PMSF; Roche), and 200 μM Na_3VO (Sigma).

For coimmunoprecipitation analysis, protein extracts (500 μg) were incubated 1 h 4 °C with 2 μg of rabbit polyclonal anti-IRS1 (sc-559 SANTACRUZ, Santa Cruz, CA, USA) or rabbit polyclonal anti-IRS2 (sc-8299, SANTACRUZ), followed by an incubation (1 h, 4 °C) with 30 μL of 50% Protein A/G PLUS-Agarose (sc-2003, SANTACRUZ). Beads were washed twice (16 000 g, 5 s) with TNG buffer for IRS1 immunoprecipitation or with CLB buffer (2.5 mM Tris-HCl, 150 mM NaCl, 1 mM EDTA, 1 mM EGTA and 1% Triton X100) for IRS2 immunoprecipitation. Immunoglobulin–protein complexes were eluted from beads by boiling in Laemmli's buffer (30 μL) and were subjected to 8% polyacrilamide gel electrophoresis and western blot analysis.

For whole protein analysis, protein extracts (50–250 μg) were analyzed by 12% polyacrilamide gel electrophoresis (for analysis of the insulin-signaling proteins) or 15% polyacrilamide gel electrophoresis (for *Ink4/Arf* proteins analysis) followed by western blot (Gonzalez-Navarro *et al.*, 2008).

The following primary antibodies were used for the western blot analysis: rabbit anti-SAPK/JNK (56G8) (1/500, 9258, Cell Signaling, Danvers, MA, USA), rabbit anti-phospho-SAPK/JNK (Thr183/Tyr185) (1/500 2994, Cell Signaling), rabbit polyclonal IgG anti-phospho-Akt (Ser473) (1/250, 9271 Cell Signaling), goat polyclonal IgG anti-Akt1/2 (1/1000, sc-1619), mouse anti-phospho-Tyr (1/500, clon 4G10, 05-321, UPSTATE, Millipore, Madrid, Spain), rabbit anti-p85α (1/500, 06-195, UPSTATE), rabbit anti-IRS2 (1/200, 06-506, UPSTATE), rabbit anti-IRS1 (1/1000, 2382 Cell Signaling), rabbit anti-$p16^{ink4a}$ and anti-$p19^{Arf}$ (1/200, sc-1207 and sc-32748, respectively, SANTACRUZ), rabbit anti-$p15^{ink4b}$ (1/500, 4822 Cell Signaling), and mouse anti-β-actin (1/500, A5441, Sigma). HRP conjugated secondary antibodies (1/300) from SANTACRUZ were as follows: anti-mouse IgG-HRP (sc-2031), goat anti-rabbit IgG-HRP (sc-2004), and donkey anti-goat IgG-HRP (sc-2056). Immunocomplexes were detected with ECL Plus detection kit (GE Healthcare, ThermoFisher, Barcelona, Spain). For quantification of protein levels, we performed densitometry scanning of protein bands. Expression levels in bar graphs are shown relative to unphosphorylated

forms of the protein or to β-actin for total protein extracts in Western blots, and to unstimulated protein levels in coimmunoprecipitations assays.

Gene expression analysis by quantitative real-time PCR (qPCR)

RNA from liver, skeletal muscle, heart, and isolated pancreatic islets (50–80 islets per sample) of 1-year-old mice was obtained using TRIzol Reagent (Invitrogen, Life Technologies, Madrid, Spain) and a homogenizer. RNA purity and concentration were determined by the A260/280 ratio, and RNA (0.5–1 μg) was retrotranscribed and amplified with SuperScript III First Strand Synthesis Supermix and Platinum SYBR Green qPCR Supermix-UDG with Rox dye (Invitrogen). Reactions were run on a thermal Cycler 7900 Fast System (liver and heart: 1 cycle of 95 °C 10 min, 40 cycles 95 °C 15 s, 60 °C 1 min; isolated islets and skeletal muscle: 1 cycle of 95 °C 10 min, 50 cycles 95 °C 15 s, 60 °C 1 min), and results were analyzed with the software provided by the manufacturer (Applied Biosystems, Life Technologies). The following primers (Forward: Fw; Reverse: Rv) were used: *cyclophilin* (Fw: 5′ TGGAGAGC ACCAAGACAGACA-3′ and Rv 5′-TGCCGGAGTCGACAATGAT-3′); *irs1* (Fw: 5′-CGGAGAGCGATGGCTTCTC-3′ and Rv: 5′-GTTTGTGCATGCTCT TGGGTTT-3′); irs2 (Fw: 5′-CGGTCGACTGCTGTCT GAAC-3′ and Rv: 5′-GAGGGCGATCAGGTACTTGTG-3′). $p15^{Ink4b}$ (Fw 5 ′-AGATCCCAAC-GCCCTGAAC-3′ and Rv 5′-CCCATCATCATGACCTGG ATT-3′); $p16^{Inka}$ (Fw:5′-CGTACCCCGATTCAGGTGAT-3′; Rv: 5′-TTGAG CAGAAGAGCT GCTACGT-3′); and $p19^{Arf}$ (Fw:5′-TCTTGAGAAGAGGGCCGCACC-3′ and Rv:5′-GAATCTGCACCGTAGTTGAGC-3′).

Apoptosis analysis in bone-marrow-derived macrophages

Bone-marrow-derived macrophages were obtained from femoral bone marrow and differentiated (1×10^6 cells/mL) 7 days in DMEM P/S, 10% fetal bovine serum and 10% L929-cell conditioned medium (as a source of macrophage colony-stimulating factor). To induce apoptosis, macrophages were exposed to ultraviolet light (80 J/m^2). After 24 h, cells were trypsinized, collected by centrifugation (5 min, 400 g), fixed with 80% ethanol (30 min, −20 °C), and labeled 30 min at room temperature with propidium iodide solution (50 μg/mL, RNase A, 0.025 mg/mL). Apoptotic hypodiploid cells were detected by flow cytometry (FACSCanto, BD Biosciences, Madrid, Spain) .

Statistical analysis

Data are presented as mean ± SEM. Differences among groups were evaluated by Student's *t*-test (GraphPad Prism Software, Inc, La Jolla, CA, USA) or one-way ANOVA with Fisher's post hoc test (Statview, SAS institute, Cary, USA). F-test was used for regression analysis. Outliers identified by Grubb's test were not considered for quantification. Statistical significance was taken at $P < 0.05$.

Acknowledgments

We thank M. J. Andrés-Manzano for help with figure preparation and L. Nuñez for excellent technical assistance. Work supported by grants from the Spanish Ministry of Economy and Competiveness (MINECO) and European Regional Development Fund (SAF2007-62110, SAF2010-16044, SAF2008-0011, SAF2011-23777), and from the Instituto de Salud Carlos III (FIS: PI-CP10/00555, RECAVA: RD06/0014/0021, and EMER07-12). H.G.-N. is an investigator from 'Miguel Servet' programme (CP10/00555) and A.V. from MINECO. The Centro Nacional de Investigaciones Cardiovasculares (CNIC) is supported by the MINECO and the Pro-CNIC Foundation.

Author contributions

HG-N conceived the study, acquisition of data, performed experiments, and wrote the manuscript; AV participated in the design of study, acquisition of data, and helped in writing the manuscript; MJS participated in some experiments and revised critically the manuscript; MD designed, performed, and analyzed PET/CT imaging studies; MAP designed and analyzed PET/CT imaging studies; MS participated in the design of the study and revised critically the manuscript; DJB participated in the design of the study, supervised experimental work, and revised critically the manuscript; VA conceived the study and wrote the manuscript.

References

Annicotte JS, Blanchet E, Chavey C, Iankova I, Costes S, Assou S, Teyssier J, Dalle S, Sardet C, Fajas L (2009) The CDK4-pRB-E2F1 pathway controls insulin secretion. *Nat. Cell Biol.* **11**, 1017–1023.

Baker DJ, Perez-Terzic C, Jin F, Pitel K, Niederlander NJ, Jeganathan K, Yamada S, Reyes S, Rowe L, Hiddinga HJ, Eberhardt NL, Terzic A, van Deursen JM (2008) Opposing roles for p16Ink4a and p19Arf in senescence and ageing caused by BubR1 insufficiency. *Nat. Cell Biol.* **10**, 825–836.

Beckman JA, Creager MA, Libby P (2002) Diabetes and atherosclerosis: epidemiology, pathophysiology, and management. *JAMA* **287**, 2570–2581.

Benetos A, Thomas F, Pannier B, Bean K, Jego B, Guize L (2008) All-cause and cardiovascular mortality using the different definitions of metabolic syndrome. *Am. J. Cardiol.* **102**, 188–191.

Cho H, Mu J, Kim JK, Thorvaldsen JL, Chu Q, Crenshaw EB 3rd, Kaestner KH, Bartolomei MS, Shulman GI, Birnbaum MJ. (2001) Insulin resistance and a diabetes mellitus-like syndrome in mice lacking the protein kinase Akt2 (PKB beta). *Science* **292**, 1728–1731.

Collado M, Blasco MA, Serrano M (2007) Cellular senescence in cancer and aging. *Cell* **130**, 223–233.

Consortium TWTCC (2007) Genome-wide association study of 14,000 cases of seven common diseases and 3,000 shared controls. *Nature* **447**, 661–678.

Cunnington MS, Keavney B (2011) Genetic mechanisms mediating atherosclerosis susceptibility at the chromosome 9p21 locus. *Curr. Atheroscler. Rep.* **13**, 193–201.

Doria A, Wojcik J, Xu R, Gervino EV, Hauser TH, Johnstone MT, Nolan D, Hu FB, Warram JH (2008) Interaction between poor glycemic control and 9p21 locus on risk of coronary artery disease in type 2 diabetes. *JAMA* **300**, 2389–2397.

Gan B, Hu J, Jiang S, Liu Y, Sahin E, Zhuang L, Fletcher-Sananikone E, Colla S, Wang YA, Chin L, Depinho RA (2010) Lkb1 regulates quiescence and metabolic homeostasis of haematopoietic stem cells. *Nature* **468**, 701–704.

Gil J, Peters G (2006) Regulation of the INK4b-ARF-INK4a tumour suppressor locus: all for one or one for all. *Nat. Rev. Mol. Cell Biol.* **7**, 667–677.

Gonzalez S, Serrano M (2006) A new mechanism of inactivation of the INK4/ARF locus. *Cell Cycle* **5**, 1382–1384.

Gonzalez-Navarro H, Vila-Caballer M, Pastor MF, Vinue A, White MF, Burks D, Andres V (2007) Plasma insulin levels predict the development of atherosclerosis when IRS2 deficiency is combined with severe hypercholesterolemia in apolipoprotein E-null mice. *Front. Biosci.* **12**, 2291–2298.

Gonzalez-Navarro H, Vinue A, Vila-Caballer M, Fortuno A, Beloqui O, Zalba G, Burks D, Diez J, Andres V (2008) Molecular mechanisms of atherosclerosis in metabolic syndrome: role of reduced IRS2-dependent signaling. *Arterioscler. Thromb. Vasc. Biol.* **28**, 2187–2194.

Gonzalez-Navarro H, Abu Nabah YN, Vinue A, Andres-Manzano MJ, Collado M, Serrano M, Andres V (2010) p19(ARF) deficiency reduces macrophage and vascular smooth muscle cell apoptosis and aggravates atherosclerosis. *J. Am. Coll. Cardiol.* **55**, 2258–2268.

Gurumurthy S, Xie SZ, Alagesan B, Kim J, Yusuf RZ, Saez B, Tzatsos A, Ozsolak F, Milos P, Ferrari F, Park PJ, Shirihai OS, Scadden DT, Bardeesy N (2010) The Lkb1 metabolic sensor maintains haematopoietic stem cell survival. *Nature* **468**, 659–663.

Hamsten A, Eriksson P (2008) Identifying the susceptibility genes for coronary artery disease: from hyperbole through doubt to cautious optimism. *J. Intern. Med.* **263**, 538–552.

Hirosumi J, Tuncman G, Chang L, Gorgun CZ, Uysal KT, Maeda K, Karin M, Hotamisligil GS (2002) A central role for JNK in obesity and insulin resistance. *Nature* **420**, 333–336.

Hotta K, Kitamoto A, Kitamoto T, Mizusawa S, Teranishi H, So R, Matsuo T, Nakata Y, Hyogo H, Ochi H, Nakamura T, Kamohara S, Miyatake N, Kotani K, Komatsu R, Itoh N, Mineo I, Wada J, Yoneda M, Nakajima A, Funahashi T, Miyazaki S, Tokunaga K, Masuzaki H, Ueno T, Chayama K, Hamaguchi K, Yamada K, Hanafusa T, Oikawa S, Yoshimatsu H, Sakata T, Tanaka K, Matsuzawa Y, Nakao K, Sekine A (2012) Association between type 2 diabetes genetic susceptibility loci and visceral and subcutaneous fat area as determined by computed tomography. *J. Hum. Genet.* **57**, 305–310.

Hribal ML, Presta I, Procopio T, Marini MA, Stancakova A, Kuusisto J, Andreozzi F, Hammarstedt A, Jansson PA, Grarup N, Hansen T, Walker M, Stefan N, Fritsche A, Haring HU, Pedersen O, Smith U, Laakso M, Sesti G (2011) Glucose tolerance, insulin sensitivity and insulin release in European non-diabetic carriers of a polymorphism upstream of CDKN2A and CDKN2B. *Diabetologia* **54**, 795–802.

Janzen V, Forkert R, Fleming HE, Saito Y, Waring MT, Dombkowski DM, Cheng T, DePinho RA, Sharpless NE, Scadden DT (2006) Stem-cell ageing modified by the cyclin-dependent kinase inhibitor p16INK4a. *Nature* **443**, 421–426.

Kippin TE, Martens DJ, van der Kooy D (2005) p21 loss compromises the relative quiescence of forebrain stem cell proliferation leading to exhaustion of their proliferation capacity. *Genes Dev.* **19**, 756–767.

Krishnamurthy J, Torrice C, Ramsey MR, Kovalev GI, Al-Regaiey K, Su L, Sharpless NE (2004) Ink4a/Arf expression is a biomarker of aging. *J. Clin. Investig.* **114**, 1299–1307.

Krishnamurthy J, Ramsey MR, Ligon KL, Torrice C, Koh A, Bonner-Weir S, Sharpless NE (2006) p16INK4a induces an age-dependent decline in islet regenerative potential. *Nature* **443**, 453–457.

Kuo C-L, Murphy AJ, Sayers S, Li R, Yvan-Charvet L, Davis JZ, Krishnamurthy J, Liu Y, Puig O, Sharpless NE, Tall AR, Welch CL (2011) Cdkn2a is an atherosclerosis modifier locus that regulates monocyte/macrophage proliferation. *Arterioscler. Thromb. Vasc. Biol.* **31**, 2483–2492.

Liu Y, Sanoff HK, Cho H, Burd CE, Torrice C, Mohlke KL, Ibrahim JG, Thomas NE, Sharpless NE (2009) INK4/ARF transcript expression is associated with chromosome 9p21 variants linked to atherosclerosis. *PLoS ONE* **4**, e5027.

Matheu A, Pantoja C, Efeyan A, Criado LM, Martin-Caballero J, Flores JM, Klatt P, Serrano M (2004) Increased gene dosage of Ink4a/Arf results in cancer resistance and normal aging. *Genes Dev.* **18**, 2736–2746.

Matheu A, Maraver A, Klatt P, Flores I, Garcia-Cao I, Borras C, Flores JM, Vina J, Blasco MA, Serrano M (2007) Delayed ageing through damage protection by the Arf/p53 pathway. *Nature* **448**, 375–379.

Matheu A, Maraver A, Collado M, Garcia-Cao I, Canamero M, Borras C, Flores JM, Klatt P, Vina J, Serrano M (2009) Anti-aging activity of the Ink4/Arf locus. *Aging Cell* **8**, 152–161.

Melzer D, Frayling TM, Murray A, Hurst AJ, Harries LW, Song H, Khaw K, Luben R, Surtees PG, Bandinelli SS, Corsi AM, Ferrucci L, Guralnik JM, Wallace RB, Hattersley AT, Pharoah PD (2007) A common variant of the p16(INK4a) genetic region is associated with physical function in older people. *Mech. Ageing Dev.* **128**, 370–377.

Molofsky AV, Slutsky SG, Joseph NM, He S, Pardal R, Krishnamurthy J, Sharpless NE, Morrison SJ (2006) Increasing p16INK4a expression decreases forebrain progenitors and neurogenesis during ageing. *Nature* **443**, 448–452.

Nunn AV, Bell JD, Guy GW (2009) Lifestyle-induced metabolic inflexibility and accelerated ageing syndrome: insulin resistance, friend or foe? *Nutr. Metab. (Lond)* **6**, 16.

Qian Z, Chen L, Fernald AA, Williams BO, Le Beau MM (2008) A critical role for Apc in hematopoietic stem and progenitor cell survival. *J. Exp. Med.* **205**, 2163–2175.

Ressler S, Bartkova J, Niederegger H, Bartek J, Scharffetter-Kochanek K, Jansen-Durr P, Wlaschek M (2006) p16INK4A is a robust in vivo biomarker of cellular aging in human skin. *Aging Cell* **5**, 379–389.

Rhodes CJ (2005) Type 2 diabetes-a matter of beta-cell life and death? *Science* **307**, 380–384.

Ruchat SM, Elks CE, Loos RJ, Vohl MC, Weisnagel SJ, Rankinen T, Bouchard C, Perusse L (2009) Association between insulin secretion, insulin sensitivity and type 2 diabetes susceptibility variants identified in genome-wide association studies. *Acta Diabetol.* **46**, 217–226.

Saxena R, Voight BF, Lyssenko V, Burtt NP, de Bakker PI, Chen H, Roix JJ, Kathiresan S, Hirschhorn JN, Daly MJ, Hughes TE, Groop L, Altshuler D, Almgren P, Florez JC, Meyer J, Ardlie K, Bengtsson Bostrom K, Isomaa B, Lettre G, Lindblad U, Lyon HN, Melander O, Newton-Cheh C, Nilsson P, Orho-Melander M, Rastam L, Speliotes EK, Taskinen MR, Tuomi T, Guiducci C, Berglund A, Carlson J, Gianniny L, Hackett R, Hall L, Holmkvist J, Laurila E, Sjogren M, Sterner M, Surti A, Svensson M, Svensson M, Tewhey R, Blumenstiel B, Parkin M, Defelice M, Barry R, Brodeur W, Camarata J, Chia N, Fava M, Gibbons J, Handsaker B, Healy C, Nguyen K, Gates C, Sougnez C, Gage D, Nizzari M, Gabriel SB, Chirn GW, Ma Q, Parikh H, Richardson D, Ricke D, Purcell S (2007) Genome-wide association analysis identifies loci for type 2 diabetes and triglyceride levels. *Science* **316**, 1331–1336.

Scott LJ, Mohlke KL, Bonnycastle LL, Willer CJ, Li Y, Duren WL, Erdos MR, Stringham HM, Chines PS, Jackson AU, Prokunina-Olsson L, Ding CJ, Swift AJ, Narisu N, Hu T, Pruim R, Xiao R, Li XY, Conneely KN, Riebow NL, Sprau AG, Tong M, White PP, Hetrick KN, Barnhart MW, Bark CW, Goldstein JL, Watkins L, Xiang F, Saramies J, Buchanan TA, Watanabe RM, Valle TT, Kinnunen L, Abecasis GR, Pugh EW, Doheny KF, Bergman RN, Tuomilehto J, Collins FS, Boehnke M (2007) A genome-wide association study of type 2 diabetes in Finns detects multiple susceptibility variants. *Science* **316**, 1341–1345.

Sharpless NE, DePinho RA (2007) How stem cells age and why this makes us grow old. *Nat. Rev. Mol. Cell Biol.* **8**, 703–713.

Stancakova A, Kuulasmaa T, Paananen J, Jackson AU, Bonnycastle LL, Collins FS, Boehnke M, Kuusisto J, Laakso M (2009) Association of 18 confirmed susceptibility loci for type 2 diabetes with indices of insulin release, proinsulin conversion, and insulin sensitivity in 5,327 nondiabetic Finnish men. *Diabetes* **58**, 2129–2136.

Vidal A, Koff A (2000) Cell-cycle inhibitors: three families united by a common cause. *Gene* **247**, 1–15.

Withers DJ, Gutierrez JS, Towery H, Burks DJ, Ren JM, Previs S, Zhang Y, Bernal D, Pons S, Shulman GI, Bonner-Weir S, White MF (1998) Disruption of IRS-2 causes type 2 diabetes in mice. *Nature* **391**, 900–904.

Zeggini E, Weedon MN, Lindgren CM, Frayling TM, Elliott KS, Lango H, Timpson NJ, Perry JR, Rayner NW, Freathy RM, Barrett JC, Shields B, Morris AP, Ellard S, Groves CJ, Harries LW, Marchini JL, Owen KR, Knight B, Cardon LR, Walker M, Hitman GA, Morris AD, Doney AS, McCarthy MI, Hattersley AT (2007) Replication of genome-wide association signals in UK samples reveals risk loci for type 2 diabetes. *Science* **316**, 1336–1341.

Zhang J, Grindley JC, Yin T, Jayasinghe S, He XC, Ross JT, Haug JS, Rupp D, Porter-Westpfahl KS, Wiedemann LM, Wu H, Li L (2006) PTEN maintains haematopoietic stem cells and acts in lineage choice and leukaemia prevention. *Nature* **441**, 518–522.

Zindy F, Quelle DE, Roussel MF, Sherr CJ (1997) Expression of the p16INK4a tumor suppressor versus other INK4 family members during mouse development and aging. *Oncogene* **15**, 203–211.

Supporting Information

Additional Supporting Information may be found in the online version of this article at the publisher's web-site.

Figure S1. Increased gene dosage of *Ink4/Arf* does not affect pancreatic islet number and area or β-cell proliferation in 1-year-old mice.